

PAPER • OPEN ACCESS

## Comparison of laboratory grating-based and speckle-tracking x-ray phase-contrast imaging

To cite this article: J. Romell *et al* 2017 *J. Phys.: Conf. Ser.* **849** 012035

View the [article online](#) for updates and enhancements.

### Related content

- [Reconstruction method for grating-based x-ray phase-contrast images without knowledge of the grating positions](#)  
G. Pelzer, J. Rieger, C. Hauke et al.
- [Visibility in differential phase-contrast imaging with partial coherence source](#)  
Liu Xin, Guo Jin-Chuan, Peng Xiang et al.
- [Reconstruction of In-Line Holograms Using Phase Retrieval Algorithms](#)  
Yan Zhang, Giancarlo Pedrini, Wolfgang Osten et al.

# Comparison of laboratory grating-based and speckle-tracking x-ray phase-contrast imaging

J. Romell<sup>1</sup>, T. Zhou<sup>1</sup>, M. Zdora<sup>2,3</sup>, S. Sala<sup>2,3</sup>, F.J. Koch<sup>4</sup>, H.M. Hertz<sup>1</sup>, A. Burvall<sup>1</sup>

<sup>1</sup> Biomedical and X-ray Physics, KTH Royal Institute of Technology, AlbaNova University Center, SE-106 91, Stockholm, Sweden

<sup>2</sup> Diamond Light Source, Harwell Science & Innovation Campus, Didcot, Oxfordshire OX11 0DE, UK

<sup>3</sup> Department of Physics & Astronomy, University College London, London WC1E 6BT, UK

<sup>4</sup> Institute of Microstructure Technology, Karlsruhe Institute of Technology, 76344 Eggenstein-Leopoldshafen, Germany

E-mail: [jenny.romell@biox.kth.se](mailto:jenny.romell@biox.kth.se)

**Abstract.** Phase-contrast imaging with x-rays is a developing field for imaging weakly absorbing materials. In this work, two phase-contrast imaging methods, grating- and speckle-based imaging, that measure the derivative of the phase shift, have been implemented with a laboratory source and compared experimentally. It was found that for the same dose conditions, the speckle-tracking differential phase-contrast images have considerably higher contrast-to-noise ratio than the grating-based images, but at the cost of lower resolution. Grating-based imaging performs better in terms of resolution, but would require longer exposure times, mainly due to absorption in the grating interferometer.

## 1. Introduction

To overcome the limitations of low resolution and poor contrast when imaging weakly absorbing objects with x-rays, different phase-sensitive imaging techniques are being developed. While conventional absorption is readily measured, phase shift must be detected by finding the intensity variations caused by the shift. The well-established propagation-based imaging method (PBI) measures the second-order derivative of the phase, while grating-based imaging (GBI) [1] and the relatively new speckle-based imaging (SBI) [2, 3] measure the refraction angle. By tracking the shift of a known intensity pattern, a map of the refraction angle, which is proportional to the derivative of the phase shift, can be constructed. GBI and SBI use a Talbot pattern [4] and a near-field speckle pattern, respectively. These two methods have been implemented with a laboratory micro-focus x-ray source, and have been used to image different samples under the same dose conditions, with the goal of comparing the quality of the obtained images.

## 2. Method

The experimental arrangements of grating- and speckle-based imaging are shown in Fig. 1. The liquid-metal-jet source, similar to the source described in [5], was run at 40 kVp with an emission current of 0.6 mA, generating an x-ray beam with spot size  $5.3 \times 7.7 \mu\text{m}^2$ . To keep the dose controlled, the source-to-object distance was kept constant at 65.6 cm at all times. The grating



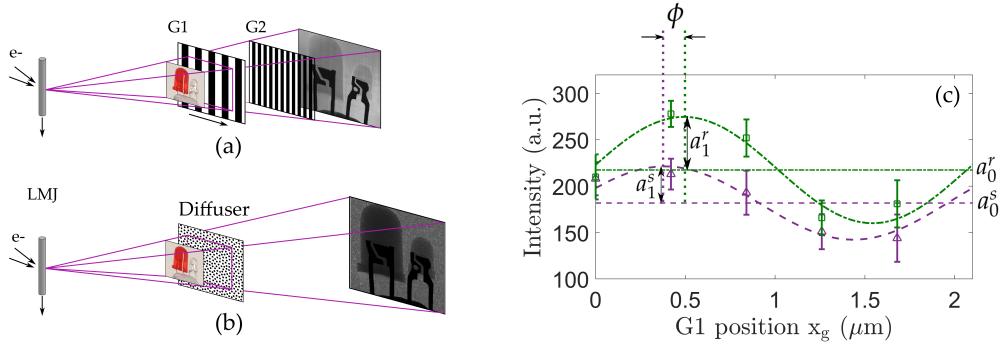


**Figure 1.** Experimental arrangements. (a) GBI. (b) SBI. (c) The intensity of a pixel during phase stepping in the GBI method, where deviations from the fit indicate photon noise.

interferometer used in GBI was designed with grating periods  $p_1 = 4.08 \mu\text{m}$  of the  $\pi$ -shifting phase grating G1 and  $p_2 = 2.4 \mu\text{m}$  of the absorption grating G2. Si with a thickness of  $200 \mu\text{m}$  was used as substrate for both gratings, with  $9.2 \mu\text{m}$  of Ni on G1 and  $40 \mu\text{m}$  of gold on G2. Both G1 and G2 had a duty cycle of 50%. The distance between the gratings was  $d = 12.4 \text{ cm}$ , and the detector was placed as close as possible after G2. For SBI, the speckle pattern was generated by a diffuser, here a piece of P800 sandpaper, placed after the sample. To reach sufficient speckle visibility [6], the detector was placed 1.5 m away from the source.

In GBI, G1 was scanned laterally over one period of the Talbot intensity pattern [1]. For each step, two images were recorded: one with a sample in the beam path, and one reference without. Processing of the stacks of images was carried out pixel-wise. The intensity variation of one pixel during the phase stepping can be seen in Fig. 1c, and can be described in terms of a cosine series. The superscripts  $s$  and  $r$  denote *sample* and *reference*, respectively. Differential phase contrast (DPC), which has been the main interest in this work, is proportional to  $\phi = \phi_1^s - \phi_1^r$ . For the grating interferometer, the angle of refraction  $\alpha$  is related to the phase shift  $\Phi(x, y)$  caused by the object, and to  $\phi$  as [7]

$$\alpha_x = \frac{\partial \Phi}{\partial x} \frac{\lambda}{2\pi} = \frac{\phi p_2}{2\pi d}. \quad (1)$$

The parameters  $a_0$ ,  $a_1$  and  $\phi_1$ , for both reference and sample, were extracted from the raw images by fast Fourier transform.

In x-ray speckle-tracking imaging, the type of SBI considered here, two images were recorded: one with only the diffuser in the beam path, and one with the diffuser and the sample. The arrangement is shown in Fig. 1b. Since no scanning process was carried out, the images were compared region-wise to find the shift of the speckle pattern, the absorption, and the loss of speckle visibility. Least-square minimisation of a cost function [8] gave the sample-induced local shift  $(\delta_x, \delta_y)$  around each pixel, in both horizontal and vertical directions. For comparison with GBI, only the horizontal shift has been considered. From the shift, the angles of refraction could be calculated as  $\alpha_i = \delta_i/L$  for  $i = x, y$ , where  $L$  is the diffuser-to-detector distance. The resolution in the final images was mainly affected by the window size chosen for the reconstruction.

### 3. Results

For a plastic wedge with a small angle, specifically a LEGO<sup>®</sup> sword (Fig. 2), the contrast-to-noise ratios (CNR) of the DPC images were evaluated as  $\text{CNR} = |I_A - I_B|/\sigma$ . Here,  $\sigma$  is the standard deviation of the background and  $I$  the mean intensity. The figure was imaged with GBI and SBI for an exposure time of 540 s each, and for the SBI reconstruction a  $24 \times 24$  pixel window

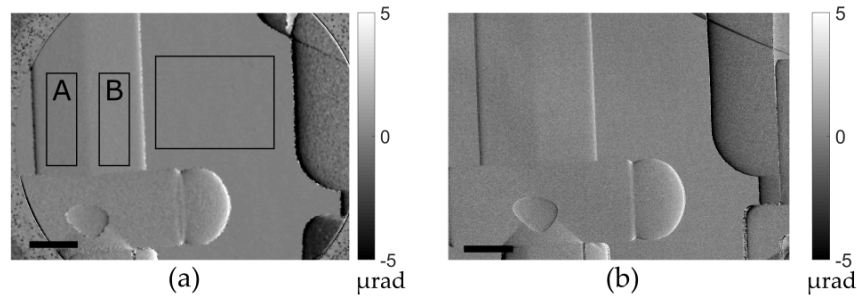


**Figure 2.** DPC images, expressed as refraction angle  $\alpha_x \propto \partial\Phi/\partial x$ . (a) SBI, with regions used in the CNR calculation. (b) GBI. The scale bar represents 2 mm in both figures.

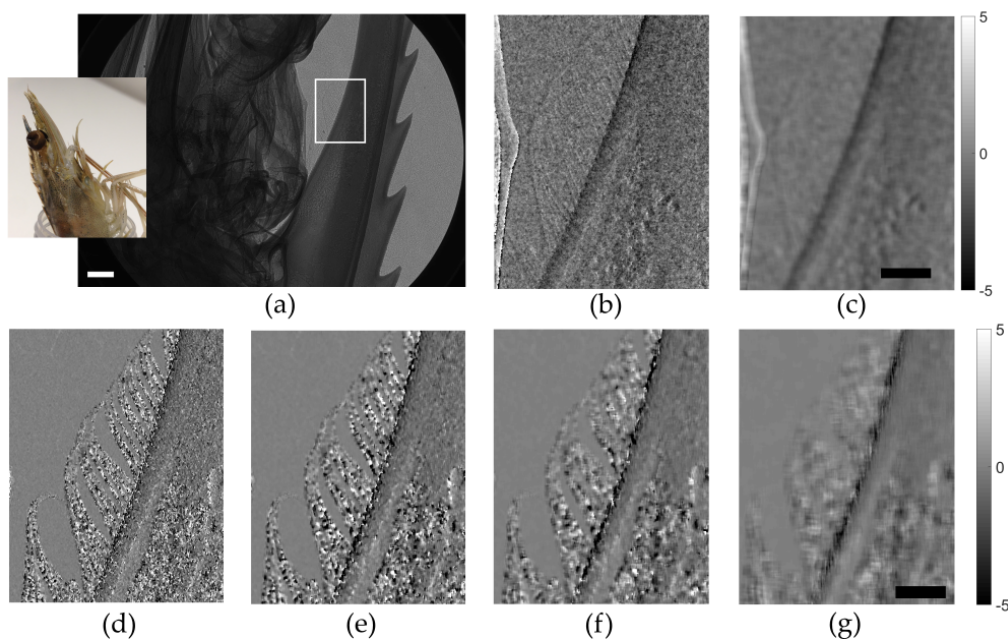


**Figure 3.** (a) Shrimp with marked region used for the DPC images (b)–(g). (b) GBI differential phase contrast. (c) Low-pass filtered GBI. (d)–(g) Speckle-based images, reconstructed with a window of  $N \times N$  pixel<sup>2</sup>, where  $N$  is (d) 4, (e) 8, (f) 12 and (g) 24. The white scale bar corresponds to 1 mm and the black 500  $\mu\text{m}$ . The grey scale represents refraction angle in  $\mu\text{rad}$ .

was chosen for optimal noise [8]. Partly due to the inherent filtering in the speckle-tracking reconstruction method, the CNR was here 9.6, compared to 0.83 of GBI.

To evaluate the resolution, some small structures on a shrimp (see Fig. 3a) were imaged. The exposure time was 780 s. Since the window size of the SBI reconstruction greatly impacts not only noise but also resolution, different window sizes  $N \times N$  pixel<sup>2</sup> were used,  $N$  ranging from 4 to 24. Shown in Fig. 3d-g are reconstructions for  $N = 4, 8, 12$  and 24. It is clear from considering Fig. 3g that choosing a large window will filter out small features, while the hairs could be clearly seen, however noisy, when a window of  $8 \times 8$  or  $4 \times 4$  pixel<sup>2</sup> was used. The GBI DPC image, acquired during the same exposure time (Fig. 3b), showed strong background noise which made it difficult to distinguish the hairs at all. Comparing the methods from a noise perspective, by low-pass filtering the GBI image until the same background noise as in the  $4 \times 4$  speckle image was reached (Fig. 3c), showed that the hairs were then blurred out entirely.

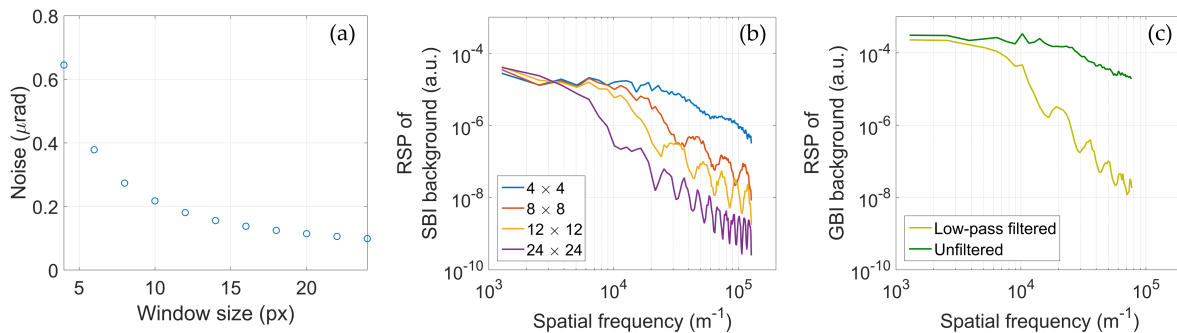


**Figure 4.** (a) Background noise of SBI DPC reconstructions of the shrimp (Fig. 3a) as a function of the window size. (b) Background RSP for SBI. (c) Background RSP for GBI.

Noise is clearly limiting the detectability of small features in the grating-produced image, while the reconstruction window, and hence resolution, is the main limiting factor for the speckle-tracking method. The noise dependence on the reconstruction window was evaluated by determining the background noise for different window sizes (Fig. 4a).

Finally, to appreciate the impact of the reconstruction method on the images, the average radial spectral power (RSP) of the background was evaluated for the four different window sizes used in Figs. 3d-g, and the unfiltered and filtered GBI from Figs. 3b and 3c. The RSP is shown in Figs. 4b and 4c. The effect of the rectangular window can clearly be seen in the fluctuations in Fig. 4b and the filtered GBI in Fig. 4c.

#### 4. Conclusion and outlook

To summarise, the quality of the DPC images largely depends on both experimental arrangement and reconstruction method. The speckle-tracking method gives considerably higher CNR than GBI, but at the cost of lower resolution. With GBI, smaller details can be resolved, but it requires a larger dose, mainly due to the absorption in the interferometer.

As a continuation of this work, image quality in GBI could be compared to variations of SBI which can give higher resolution, such as speckle-scanning phase-contrast imaging.

#### Acknowledgments

We thank William Vågberg and Jakob Larsson for assistance in the lab, and Karlsruhe Institute of Technology (KIT) for providing the gratings for the interferometer.

#### References

- [1] Pfeiffer F, Weitkamp T, Bunk O and David C 2006 Phase retrieval and differential phase-contrast imaging with low-brilliance X-ray sources *Nat. Phys.* **2** pp 258–61
- [2] Morgan K S, Paganin D M and Siu K K W 2012 X-ray phase imaging with a paper analyzer *App. Phys. Lett.* **100** 124102
- [3] Bérubon S, Ziegler E, Cerbino R, Peverini L 2012 Two-Dimensional X-Ray Beam Phase Sensing *Phys. Rev. Lett.* **108** 158102
- [4] Talbot H F 1836 Facts related to optical science *Philos. Mag.* **9** pp 401–7
- [5] Larsson D H *et al.* 2011 A 24 keV liquid-metal-jet x-ray source for biomedical applications *Rev. Sci. Instrum.* **82** 123701
- [6] Zhou T *et al.* 2015 Speckle-based x-ray phase-contrast imaging with a laboratory source and the scanning technique *Opt. Lett.* **40** pp 2822–5
- [7] Bech M 2009 *X-ray imaging with a grating interferometer*, PhD thesis, University of Copenhagen
- [8] Zanette I *et al.* 2014 Speckle-based x-ray phase-contrast and dark-field imaging with a laboratory source *Phys. Rev. Lett.* **112** 253903